



Implications of Axial Displacement on the Stacked Ring Configuration of Permanent Magnetic Bearings (PMB) in a Horizontal Overhung System

Azman Jamaludin¹, Mohd. Zarhamdy Md Zain^{1,*}, Nur Safwati Mohd Nor¹

¹ Fakulti Kejuruteraan Mekanikal, Universiti Teknologi Malaysia, 81310 Skudai, Johor, Malaysia

ARTICLE INFO

Article history:

Received 21 November 2025

Received in revised form 10 January 2026

Accepted 15 January 2026

Available online 31 January 2026

ABSTRACT

In a horizontal overhung system, a stacked ring configuration of Permanent Magnetic Bearings (PMB) demonstrated axial instability and a noticeable sensitivity to geometric imperfections. Backer's research model allows for the study of the effect of maximum radial displacement, yet it struggles to resolve issues with establishing stiffness for axial displacement. Since then, various models have been employed to bridge the gaps in understanding axial stiffness. While there has been extensive research into stacked ring configurations for horizontal overhung systems, existing designs commonly exhibit poor axial stiffness, which causes excessive rotor movement, inherent instability, and restricts their applicability. Most studies indicate that axial instability can be mitigated through the use of bearing supports, such as electro-mechanical servo mechanisms, but further knowledge is required to optimise design parameters for effective axial displacement control. Therefore, there is a critical need to develop a novel PMB configuration that maximises axial stiffness while minimising reliance on bearing supports for axial displacement management. A rotor system is constructed incorporating an N35 grade axially magnetized neodymium magnet within a cartridge assembly, along with a rotating shaft sleeve and setting plates designed for a non-metallic steel forging step shaft. The innovative hybrid overhung rotor design includes a durable marine-grade thrust bearing housing and a split industrial Plummer block housing, engineered to house a set of C3 angular contact ball bearings. Results from experiments revealed a stable linearity of air gaps for the range of ring thickness-wavelength ratio d/λ size up to 1.06. Conversely, the reverse effect to the ring thickness-wavelength ratio (d/λ) below 1 enhances the threshold of axial displacement. The findings indicate that axial displacement causes the magnetic wavelength (λ) to decrease by a factor of six. Furthermore, it influences the PMB's size based on the ring thickness-to-wavelength ratio (d/λ) and sustains stable PMB stiffness up to a d/λ ratio of 1.06. This stability offers an

Keywords:

Axial displacement, Air Gaps, Backers's works, Sixfold wavelength, Neodymium

* Corresponding author.

E-mail address: zarhamdy@utm.my (Mohd Zarhamdy Md Zain)

<https://doi.org/10.37934/sej.12.1.153162>

advantage in achieving an improved axial displacement threshold when the PMB thickness-to-wavelength ratio (d/λ) is less than 1.

1. Introduction

As reported by Guzmán-Mínguez et al. [4], Max Baermann substantially improved permanent magnets using plastic-bonded Alnico powder and phenolic resin, starting in the 1930s. According to the research by Wei et al. [16], Max Baermann has successfully developed a highly coercive barium ferrite powder for flexible plastics, patented for applications such as injection molding, calendaring, or extrusion. Paden et al. [12] reported that in the 1960s, F.T. Backers comprehensively reviewed Max Baermann's patented flexible magnet, which was intended for a Permanent Magnetic Bearing (PMB) model. He used a magnetic scalar potential that was based on the idea of A. H. Boerdijk for reducing friction by magnetically "floating" the shaft. Following this, multiple PMB models were created. Notably, Yu *et al.* [22] presented a review of the Coulomb method, and Yonnet [20] established a virtual work model in the 1980s. Several researchers [2,7,13,17] have noted that, although advancements have been made, such as Ravaud et al. [14] with the Coulomb method, Li. Zhang et al. [9] with the Monte Carlo model, and Tian et al. [6] on multiple solutions for axial stack permanent-magnet bearings, PMB designs still face stability issues related to radial and axial stiffness, which limit their load capacity and potential applications.

The issue of load capacity has been a subject of discussion since the 1960s, as evidenced by Baker's work. Subsequent proposals for solutions have been put forth by Yonnet [20, 21]. Furthermore, Paden et al. [12] observed in their research that enhancing stiffness, in relation to load capacity, can be achieved through the improvement of tight air gaps and the implementation of multi-thin (stacked) rings, which is a method that is proven effective in managing superior load capacities. However, introducing a multiple stacked ring would increase axial displacement and demand for PMB to have a high axial stiffness. Besides problems with stability and load capacity, multiple researchers [1,8,19] have indicated that current PMB designs do not have sufficient axial stiffness. This leads to shaft deflection, rotor-stator contact, magnet damage, and a risk of failure, as detailed by Lijesh *et al.* [5]. The findings of Baker et al. [11] suggested that active controls or stabilizers are essential for achieving balance in axial movement. Additionally, for some hybrid application configurations using PMB or conventional ball bearings as radial and thrust bearings, geometric defects affect both bearings. This exposure to defects can lead to rotor instability caused by axial displacement issues, a concern highlighted by multiple authors in the context of conventional machines [10,13,16,18,19]. As specified by Backer, a small axial deviation in PMB needs to be managed. To achieve optimized axial stiffness with reduced dependence on active control systems and bearing support as described by Baker, a new PMB configuration needs to be developed to meet the axial displacement threshold.

2. Methodology

2.1 Mathematic Model

Baker developed a theoretical model of a two-plate system as illustrated in Figure 1(a), where two parallel magnetic plates are positioned with an air gap with a distance of h_0 between them. According to Reimann *et al.* [15], a time-varying magnetic field, with an estimated wavelength of λ_0 , will create an interaction between the plates in the Z direction, inducing precession in their magnetic moments. The two plates interact via their dipolar fields in the N-S-S-N configuration. Baker described that the influence of the wave, determined by the wavelength, dictates the spatial distribution of the

magnetic moment as described in Eq. (1). The magnetic moment for plate 1 is defined as $M_1 = M_0 \cdot \cos(2\pi(z)/\lambda_0)$, while for plate 2, $M_2 = M_0 \cdot \cos(2\pi(z+z_0)/\lambda_0)$, where phase shift captured by displacement at z_0 .

$$\sigma = \left(\frac{M_1 M_2}{2\mu_0}\right) \left(1 - \frac{1}{e^{\left(\frac{2\pi d}{\lambda_0}\right)}}\right)^2 \left(\frac{1}{e^{\left(\frac{2\pi h_0}{\lambda_0}\right)}}\right) \quad (1)$$

As illustrated in Figure 1(b), plate 1 experienced a displacement of ΔL along the Z direction, resulting in a modified two-plate interaction with a shorter wavelength λ .

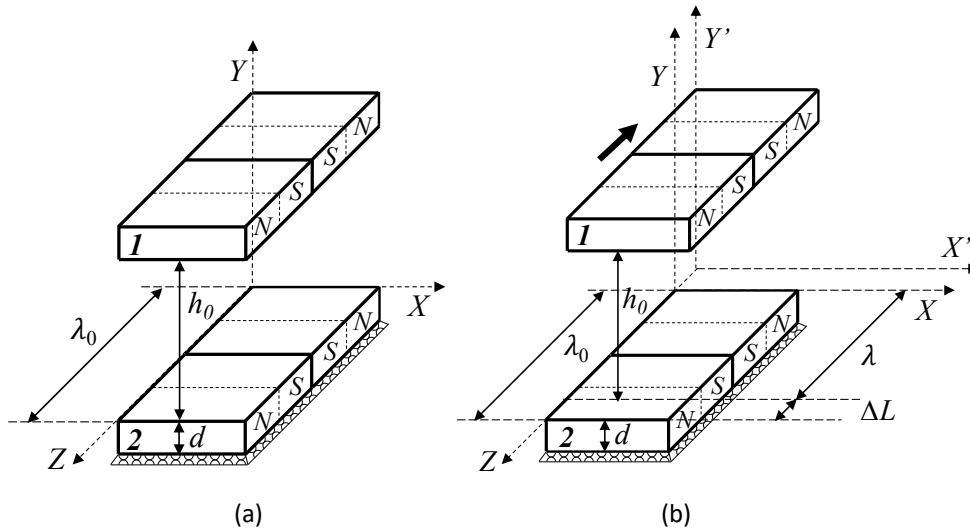


Fig. 1. Two-plate system: (a) without axial displacement, (b) with axial displacement

According to Yonnet *et al.* [21,22], evaluating the intersection reveals that a magnet with the same strength can reverse in another direction. Region 2 has the same magnetic strength as region 3 in the opposite direction. Similar magnetism occurs in Regions 4 and 5. Figure 2 reveals that a combination of “null” magnetisation interfaces for areas 1 and 6, and areas 2, 3, 4, and 5, leads to a reduction in the initial wavelength and a zero six-fold axial displacement.

In a fully stacked ring PMB, the plates are shaped based on *the* ratio of ring thickness to wavelength (d/λ) as well as the inner (r_1) and outer (r_2) ring radii. According to Bakers and Paden *et al.* [12], the ring’s radial displacement aligns with the peak of magnetic pressure at an eccentricity $e = h_0$ [3,4]. The connection between eccentricity and the air gaps h_0 and h_1 is given by the equation $h_1 = h_0 - e \cdot \cos\theta$ [4].

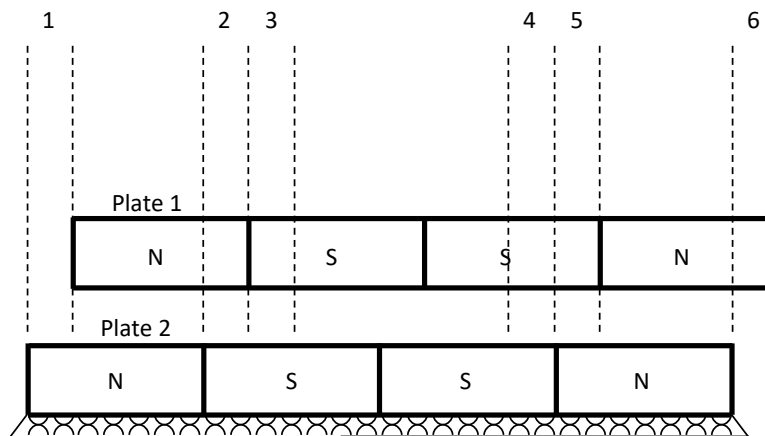


Fig. 2. Stacked ring magnet misalignment between N-S-S-N between plate 1 and plate 2

Eq. (1) is then integrated over $r = (r_2 - r_1) / 2$ and angle θ to obtain the repulsive force (F_m) on PMB rotor, where $P_m = F/2\lambda r$, and M_1 and M_2 are periodic functions represented by Fourier series representations for infinite sum of $m \in \{1, 2, 3, \dots, \infty\}$ and $n \in \{1, 2, 3, \dots, \infty\}$. By decomposing the function into a weighted sum on $[-\lambda/2, \lambda/2]$, Eq. (2) calculates the magnetic pressure (P_m) between the outer and inner rings.

$$P_m = \frac{4M_1M_2}{\mu_0} \sum_{n=1,3,5,7,\dots}^{\infty} \left(\frac{\left(\frac{1}{e^{\left(\frac{n2\pi h_1}{\lambda} \right)}} \right) \left(1 - \frac{1}{e^{\left(\frac{n2\pi d}{\lambda} \right)}} \right)^2 I \left(\frac{n2\pi(e)}{\lambda} \right)}{n^2} \right) \quad (2)$$

2.2 Material and Instrument

An axially magnetised N35 neodymium magnet features a residual magnetism (Br) of 117,000 gauss (G), a coercive force of 10.8 kOe, and an energy product of 33 MGOe. The 304 stainless steel cartridge includes a rotating shaft sleeve and adjustment plates that separate the stator from the rotating rings. The shaft is built of $\varnothing 64$ mm round-rolled non-metallic steel forgings complying to marine-grade standards (DIN 1.4401, X5CrNiMo17-12-2, 316S16, Z6CND17.11, SUS316, and 2347) to withstand bending moments and torque. Furthermore, the FAG SAV 890 split Plummer block thrust bearing housing is made of two pieces of cast iron and is designed for mounting on a through-shaft. It uses NTN7210B angular contact ball bearings. As a general guideline, these bearings should be replaced when their clearance reaches 140% to 150% of the manufacturer's maximum initial specified clearance, which is 0.4 mm. Figure 3 shows a 600 x 400-mm aluminium base skid with a 10-mm thickness. Different axial displacements ($\Delta L_0, \Delta L_A, \Delta L_B, \Delta L_C, \Delta L_D, \Delta L_E, \Delta L_F, \Delta L_G,$ and ΔL_H) will lead to varied stress distributions in the stacked ring PMB. Casio DQD-80J thermometer can detect the temperature with $\pm 1^\circ\text{C}$ accuracy. The measurement of Air Gap (h_1) and alignments was conducted using the Insize Digital Caliper 1108-200, which provides a measuring range of 0–200 mm with an accuracy of ± 0.03 mm, as well as the Mitutoyo 500-501-10 with an accuracy of 0.05 mm. Shaft parallelism and bearing alignment assessments utilised the Shane digital dial indicator 5307 (range: 0–12.7 mm, accuracy: ± 0.03 mm) and the Mitutoyo dial gauge 513-401-10E (resolution: 0.001 mm, accuracy: ± 0.003 mm).

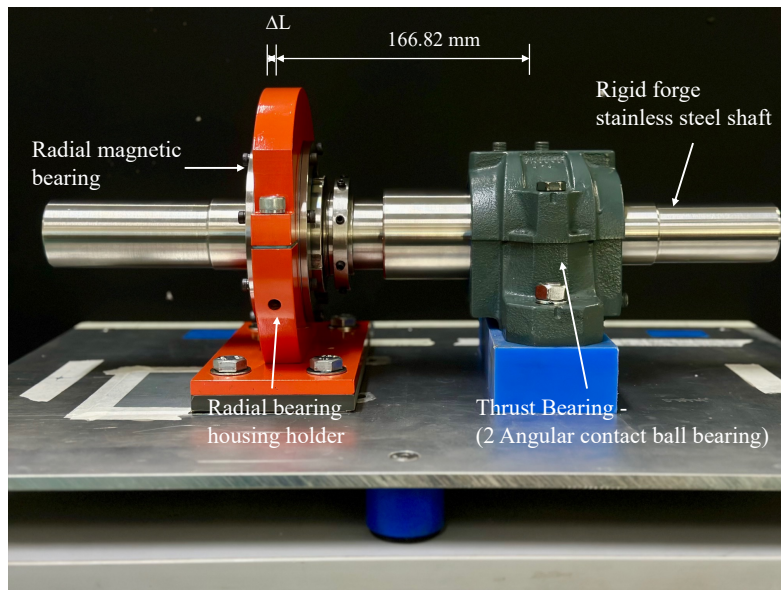


Fig. 3. The overhung rig consists of PMB set, thrust bearing and a rigid shaft

3. Result

3.1 Analytical simulation results

The model is compared with the research conducted by Zhang *et al.* [9] which employed virtual work with superposition for PMB. MATLAB is utilised to simulate various ring thickness-wavelength ratios (d/λ) of N35. Figure 4 shows that the virtual work model had an average of 0.29904, a standard deviation of 0.06112, and a standard error of the mean (SEM) of 0.0231. In comparison, the magnetic scalar potential had an average of 0.29884, a standard deviation of 0.06134, and an SEM of 0.0231. The data suggest that there is no statistically significant difference between Virtual Work and this research model (based on overlapping SEM error bars, $n=6$ per group).

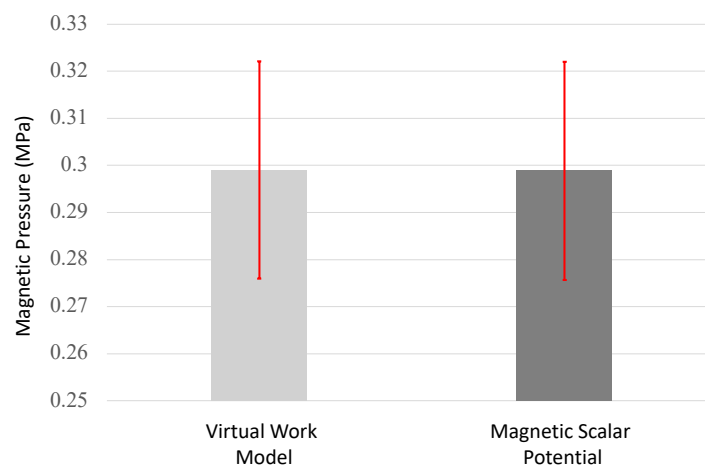


Fig. 4. Error bar for Virtual Work Model and Magnetic Scalar Potential

PMB air gap characteristics were mathematically modelled using experimental axial displacement data for $\Delta L = 0.008$ to 1.57 , with structural parameters in Figure 5. An increased axial displacement will increase the PMB's ring thickness-wavelength ratio (d/λ). Zhang *et al.* [9] explained that as the air gap narrows, magnetic pressure rises, resulting in stronger magnetic induction, greater load capacity, and a more compact PMB structure. The peak magnetic pressure (P_{mD}) reaches 0.3480 MPa when h_1 is 0.90427 mm, while the minimum magnetic pressure (P_{mH}) is 0.2965 MPa at h_1 of 0.00524 mm.

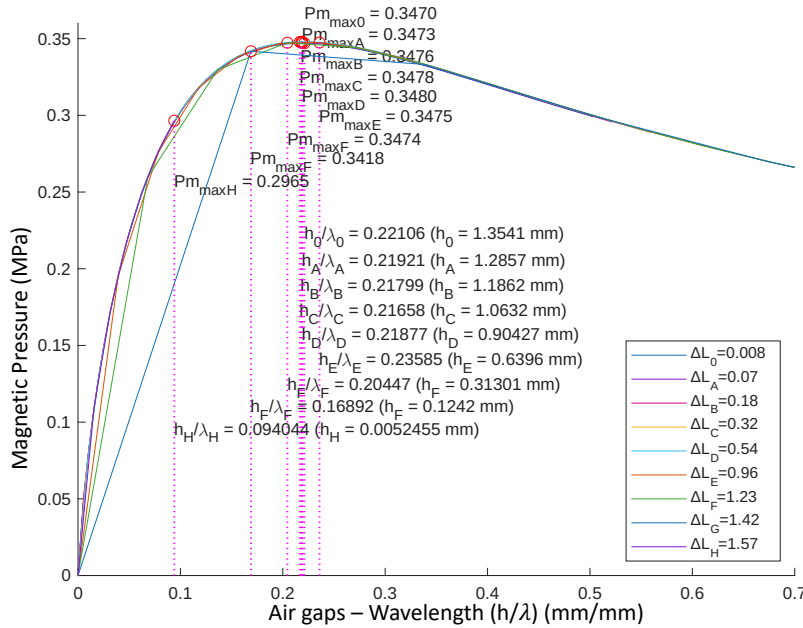


Fig. 5. Air gap and magnetic pressure model draws from the experimental data

3.2 Overall experimental result

The initial axial distance of $\Delta L_0 = 0.008$ mm is set by the thrust bearing with maximum $h_1 = 1.342$ mm and $\lambda = 9.992$ mm. The maximum axial displacement is then increased to $\Delta L_H = 1.57$ mm, resulting in $h_1 = 0$ mm and $\lambda = 8.43$ mm. Figure 5 shows that data in group 1 (ΔL_0 to ΔL_D) stayed stable and followed a linear trend, but in group 2 (ΔL_E to ΔL_H), linearity decreased.

3.3 Magnetic Pressure vs. Air Gap

In Figure 5, from ΔL_0 to ΔL_D (group 1), the ring thickness-to-wavelength ratio (d/λ) increased by 5.71% as a result of a 5.4% decrease in λ . Magnetic pressure increased by 0.29% (800 Pa), while h_1 decreased linearly by 43.20%, primarily due to the rise in magnetic pressure. For ΔL_E to ΔL_H (group 2), the ring thickness-wavelength ratio (d/λ) increased from 9.60% to 15.70%, and λ decreased similarly. In contrast to group 1, magnetic pressure decreased by as much as 14.55% (51,500 Pa), and h_1 ranged from 80.2% to 134.20%, highlighting instability due to magnetic moment loss when it exceeds 9.6%. It should be noted that, according to Baker and other sources [12, 21, 22], the ideal size of PMB used in most designs is at a ring thickness-to-wavelength ratio (d/λ) of 1. However, the maximum magnetic pressure can be achieved at a ring thickness-to-wavelength ratio (d/λ) of 1.06, which allows for a 6% increase in ring thickness compared to the wavelength.

3.4 Stiffness vs. Air Gap

The ΔL_0 to ΔL_D (group 1) PMB exhibits high stiffness, attributed to the substantial magnetic moment under load conditions. The h_1 measurements remain stable within this range until demonstrating a 28.05% decrease from their initial value. In contrast, for ΔL_E to ΔL_H (group 2), the h_1 data show instability, and PMB stiffness decreases to values below 41,283.29 N/m. As depicted in Figure 6, a reaction force of 43.365 N at the PMB corresponds to an axial displacement of 0.0011 m for ΔL_D , increasing to 0.0025 m for ΔL_F . It appears that greater stiffness in the material leads to more predictable and consistent experimental observations.

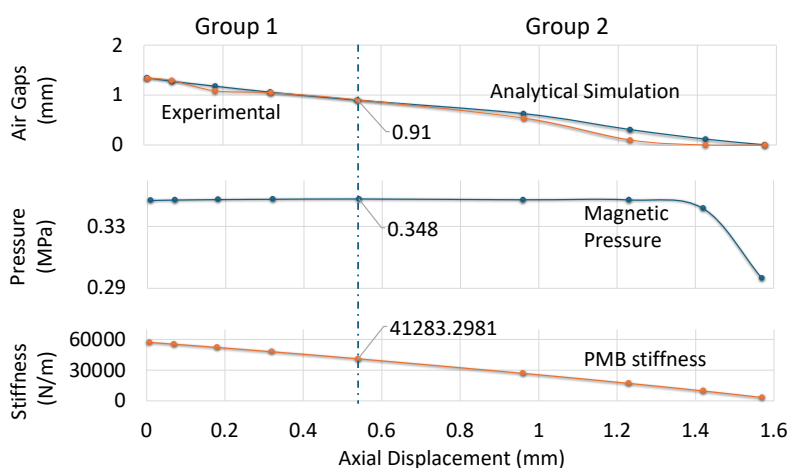


Fig. 6. Magnetic Pressure (P_m) for air gaps-wavelength ratio (h_1/λ)

3.5 Experimental vs Analytical Simulation

Figure 7 compares air gap verification across nine experimental and analytical simulations per group with statistical analysis. In group 1, experimental (average = 1.154, SD = 0.1719, SEM = 0.03601) and analytical results (average = 1.1386, SD = 0.18007, SEM = 0.0360) showed no significant difference (overlapping SEM, n = 5). In group 2, experimental (average = 0.2663, SD = 0.2731, SEM = 0.06827) and analytical results (average = 0.16, SD = 0.2576, SEM = 0.0644) differed significantly (SEM, n = 4), mainly due to spring stiffness.

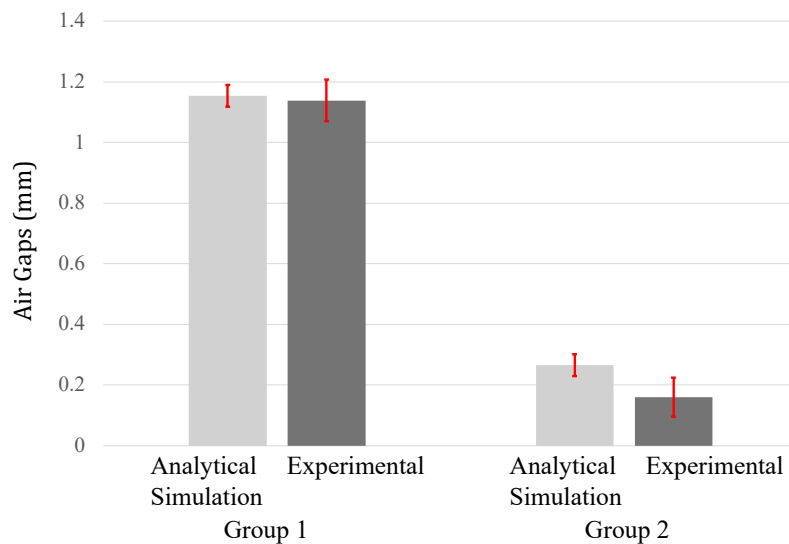


Fig. 7. Error bar group 1 and 2 for analytical simulation and experimental

4. Conclusion

This study offers a thorough evaluation and advancement of magnetic bearing technology. It draws upon numerous references and places particular emphasis on refining previous models by integrating axial displacement to optimise design. Results from experiments and analytical simulations confirmed that each axial displacement consistently leads to a sixfold reduction in magnetic wavelength, demonstrating a linear correlation with the reduction of magnetic pressure (P_m), stiffness and air gap length (h_1). Furthermore, the analysis revealed that increasing the ring thickness-wavelength ratio (d/λ) above 1 will result in a 0.3% increase in magnetic pressure (P_m). Conversely, the reverse effect to the ring thickness-wavelength ratio (d/λ) below 1 will enhance the axial displacement threshold. The experimental results indicate that the stable region's axial displacement reaches a peak of 0.54 mm with a ring thickness-to-wavelength ratio (d/λ) of 1.06, an air gap of 0.91 mm, and a maximum magnetic pressure of 0.3480 MPa. At a PMB stiffness of 41,283.29 N/m, the permissible axial displacement surpasses the typical thrust tolerance for ball bearings at a value of 0.4 mm. The research concludes that axial stiffness in PMB can be achieved by reducing the ring thickness-wavelength ratio (d/λ) to be below 1. The PMB stable axial displacement region surpasses conventional ball bearings, which will potentially reduce the need for extra support and active controllers.

Potential areas for future research include:

1. investigating the allowable axial load for 7210B angular contact ball bearings under dynamic conditions, focusing on temperature and deflection when paired with PMB, and
2. examining ways to increase axial stiffness by reducing the ring thickness-to-wavelength ratio (d/λ) below 1 in 7210B angular contact ball bearings.

Acknowledgement

The authors wish to convey profound gratitude to Universiti Teknologi Malaysia for its support. This research was not funded by any grant.

Conflict of Interest Statement

The authors declare that there is no conflict of interest regarding the publication of this paper. No financial support, grants, or other forms of compensation were received that could have influenced the outcome of this work. The research was conducted in the absence of any commercial or financial relationships that could be construed as a potential conflict of interest.

References

- [1] H. F. Asres and A. T. Kassie, "Design of Neuro Fuzzy Sliding Mode Controller for Active Magnetic Bearing Control System," *IEEE Access* 11, (2023): 103189-103200, <https://doi.org/10.1109/access.2023.3308823>
- [2] Cansız, Ahmet, İrfan Yildizer, and Daniel McGuiness. "A case study for a superconducting magnetic bearing optimization," 2017 10th International Conference on Electrical and Electronics Engineering (ELECO), Bursa, Turkey, 2017, 1466-1470. http://ieeexplore.ieee.org/xpls/abs_all.jsp?arnumber=8266280
- [3] Djaidir, Benrabeh, Ahmed Hafaifa, and Abdallah Kouzou. 2017. "Faults Detection in Gas Turbine Rotor Using Vibration Analysis Under Varying Conditions." *Journal of Theoretical and Applied Mechanics* 55, no.2, (2017): 393-406. <https://doi.org/10.15632/jtam-pl.55.2.393>
- [4] Guzmán-Mínguez, Jesús Carlos, Cecilia Granados-Mirallas, Patrick Kuntschke, César De Julián Fernández, Sergey Erokhin, Dmitry Berkov, Thomas Schliesch, Jose Francisco Fernández, and Adrián Quesada. (2023). "Remanence Increase in SrFe₁₂O₁₉/Fe Exchange-Decoupled Hard-Soft Composite Magnets Owing to Dipolar Interactions." *Nanomaterials* 13, no. 14 (2023): 2097. <https://doi.org/10.3390/nano13142097>
- [5] K.P. Lijesh, and Harish Hirani, "Development of analytical equations for design and optimization of axially polarized radial passive magnetic bearing." *Journal of Tribology* 137, no.1 (2015): 0111 3-9. <https://doi.org/10.1115/1.4028488>
- [6] L.L. Tian, X.P. Ai and Y.Q. Tian "Analytical model of magnetic force for axial stack permanent-magnet bearings." *IEEE Transactions on Magnetics* 48, (2012): 2592–2599. <https://doi.org/10.1155/2019/4265698>
- [7] Le, Yun, Di Wang, and Shiqiang Zheng. "Design and Optimization of a Radial Magnetic Bearing Considering Unbalanced Magnetic Pull Effects for Magnetically Suspended Compressor", *IEEE/ASME Transactions on Mechatronics* 27, no. 6 (2022): 5760–70. <https://doi.org/10.1109/tmech.2022.3189685>
- [8] Li, Qiang, Yefa Hu, and Huachun Wu. "Structure Design and Optimization of the Radial Magnetic Bearing." *Actuators* 12, no. 1 (2023): 27. <https://doi.org/10.3390/act12010027>
- [9] Li. Zhang, P. Hua chun, Y. Wu, H. Li and C. Song, "Design, Analysis, and Experiment of Multiring Permanent Magnet Bearings by Means of Equally Distributed Sequences Based Monte Carlo Method." *Mathematical Problems in Engineering* 1,(2019): 1-17. <https://doi.org/10.1155/2019/4265698>
- [10] McCloskey, Thomas H. 2002. "Troubleshooting Turbine Steam Path Damage Mechanisms." OakTrust (Texas a&M University Libraries), January. <https://doi.org/10.21423/r1dm1k>
- [11] Morales, Wilfredo, Robert Fusaro, and Albert Kascak. 2003. "Permanent Magnetic Bearing for Spacecraft Applications." *Tribology Transactions* 46 (3): 460–64. <https://doi.org/10.1080/10402000308982651>
- [12] Paden, Brad, Nelson Groom, and James F. Antaki. 2003. "Design Formulas for Permanent-Magnet Bearings." *Journal of Mechanical Design* 125, no.4 (2003): 734–38. <https://doi.org/10.1115/1.1625402>
- [13] Pendlebury, J. M., S. Afach, N. J. Ayres, C. A. Baker, G. Ban, G. Bison and K. Bodek "Revised Experimental Upper Limit on the Electric Dipole Moment of the Neutron." *Physical Review. D. Particles, Fields, Gravitation, and Cosmology/Physical Review. D, Particles, Fields, Gravitation, and Cosmology* 92, no. 9 (2015). <https://doi.org/10.1103/physrevd.92.092003>
- [14] Ravaud, R., G. Lemarquand, V. Lemarquand, and C. Depollier, "Discussion about the analytical calculation of the magnetic field created by permanent magnets." *Progress In Electromagnetics Research B* 11 (2009): 281-297. <https://doi.org/10.2528/PIERB08112102>
- [15] Reimann, Stephanie M., and Matti Manninen. "Electronic Structure of Quantum Dots." *Reviews of Modern Physics* 74, no. 4 (2002): 1283–1342. <https://doi.org/10.1103/revmodphys.74.1283>
- [16] Wei, Xiangxia, Ming-Liang Jin, Haiqiang Yang, Xiao-Xiong Wang, Yun-Ze Long, and Zhangwei Chen. "Advances in 3D Printing of Magnetic Materials: Fabrication, Properties, and Their Applications." *Journal of Advanced Ceramics* 11, no. 5 (2022): 665–701. <https://doi.org/10.1007/s40145-022-0567-5>
- [17] Wang, Dongxiong, Nianxian Wang, and Kuisheng Chen. 2019. "Unbalance Response of a Magnetic Suspended Dual-rotor System." *Proceedings of the Institution of Mechanical Engineers Part G Journal of Aerospace Engineering* 233, no. 15 (2019): 5758–72. <https://doi.org/10.1177/0954410019858011>
- [18] Wang, Wuchang, Yizi Shang, and Zhifeng Yao. 2022. "A Predictive Analysis Method of Shafting Vibration for the Hydraulic-Turbine Generator Unit." *Water* 14, no 17 (2022): 2714. <https://doi.org/10.3390/w14172714>

- [19] Xu, Tengfei, Lihua Yang, and Kai Wang. "Characteristics of Duplex Angular Contact Ball Bearing With Combined External Loads and Angular Misalignment." *Applied Sciences* 10, no. 17 (2020): 5756. <https://doi.org/10.3390/app10175756>
- [20] Yonnet, J. P., "Permanent magnet bearings and couplings." *IEEE Trans. Magn* 17, no. 1 (1981): 1169-1173. <https://doi:10.1109/TMAG.1981.1061166>
- [21] Yonnet, J. P., S. Hemmerlin, E. Rulliere, and G. Lemarquand, "Analytical calculation of permanent magnet couplings." *IEEE Trans. Magn* 29, no. 6 (1993): 2932-2934. <https://doi:10.1109/20.280913>
- [21] Yu.Loskutov and V. Skobelev, "Modification of the Coulomb law in a strong magnetic field." *Physics Letters A* 36, no. 5 (1971): 405-406. [https://doi.org/10.1016/0375-9601\(71\)90281-7](https://doi.org/10.1016/0375-9601(71)90281-7)